Journal of Nuclear Materials 392 (2009) 192–199

Contents lists available at ScienceDirect

Journal of Nuclear Materials

journal homepage: www.elsevier.com/locate/jnucmat

Transient hydride fuel behavior in LWRs

Kurt A. Terrani *, Jeffrey E. Seifried, Donald R. Olander

Department of Nuclear Engineering, University of California, 4155 Etcheverry Hall, M.C. 1730, Berkeley, CA 94720-1730, USA

A B S T R A C T

The transient response of a uranium zirconium hydride ($U_{0.31}ZrH_{1.6}$) fuel element to conditions typical of a light water reactor reactivity insertion accident has been studied. Hydrogen diffusion within the fuel is treated as a function of the time-dependent temperature profile. Temperature and hydrogen concentration dependence of thermal properties of the fuel is also considered. The set of coupled equations describing the transient conduction of heat and diffusion of hydrogen are solved with a Crank–Nicolson discretization scheme for heat diffusion and an explicit Euler scheme for hydrogen diffusion.

Published by Elsevier B.V.

1. Introduction

Hydride nuclear fuels (uranium–zirconium hydride) have been successfully utilized in many research and test reactors as well as space programs. The added presence of hydrogen in the fuel provides neutron moderation within the fuel in addition to the traditional moderator. This allows displacement of moderator with fuel, effectively increasing power density. Hydride fuels also enjoy a higher thermal conductivity than oxide fuels and possess thermally induced hydrogen up-scattering that accompanies Doppler feedback. Hydride fuel has also been proposed as an optimized matrix for the deep burn of plutonium and minor actinides. The proposed fuel could achieve TRU (transuranic elements) destruction fractions as high as twice that realized within MOX (mixed oxide) fuels [1].

Uranium–zirconium hydride fuel consists of metallic α-U phase dispersed in a δ-$ZrH_{1.6}$ matrix. The fuel is typically fabricated by massive hydriding of uranium zirconium alloys formed by arc melting of the metal components. Uranium inside the fuel remains metallic since the equilibrium partial pressure of the UH_3 phase at fuel processing temperatures is very high (pH_2 = 1 atm for UH_3 at ~700 K, where hydriding temperatures range from 800 to 1200 K). Maximum heavy metal loading inside the fuel is limited to 45 vol% uranium which corresponds to the fuel composition of $U_{0.31}ZrH_{1.6}$. During operation of the reactor, the temperature gradient across the fuel drives the hydrogen to the cooler regions due to the large heat of transport of hydrogen in the δ-$ZrH_{1.6}$ phase (T_Q = 640 K) [2]. Thermal conductivity of the fuel is a function of both temperature and hydrogen concentration, with a stronger dependence on the latter. The volumetric heat capacity has the same dependencies; however, its dependence on the temperature is more marked. Hydrogen diffusivity is an exponential function of temperature with a small dependence on hydrogen concentration (site blocking by other hydrogen atoms during stochastic jumps).

It is therefore necessary to couple the heat conduction to the hydrogen diffusion in order to achieve accurate results in predicting the temperature and hydrogen concentration profiles both under steady state and transient operating conditions. Accurate modeling of the coupled transient behavior will provide detailed information of the stress across the fuel as well as the necessary information for predicting the possibility of excessive hydrogen release from the fuel during accidents.

2. Methodology

2.1. Hydride fuel properties

2.1.1. Thermal conductivity and volumetric heat capacity

The fuel is a composite structure of metallic α-uranium dispersed in a δ-zirconium hydride matrix. The thermal conductivity of the fuel can be calculated as the product of thermal diffusivity, density, and specific heat capacity of the composite material. These properties can be estimated using the rule of mixtures where thermal diffusivity and density are estimated on volume fraction basis and heat capacity on mass fraction basis, respectively. Therefore the overall thermal conductivity of the fuel can be estimated using the thermal properties of uranium as a function of temperature and zirconium hydride as a function of both temperature and H/Zr ratio [3–6] as shown in Eq. (1) (Fig. 1(a)). A similar approach can be used to determine the volumetric heat capacity of the fuel as function of temperature and H/Zr ratio in the composite fuel (Fig. 1(b)). The influence of burnup on these properties is unknown and therefore this analysis is applicable only to fresh fuel. Thermal conductivity is however expected to decrease as a function of burnup since hydride fuel experiences large swelling rates, especially at low burnup conditions. Hydride fuel also has good fission gas

* Corresponding author. Tel.: +1 510 642 4077; fax: +1 510 643 9685.
E-mail address: terrani@berkeley.edu (K.A. Terrani).

0022-3115/$ - see front matter Published by Elsevier B.V.
doi:10.1016/j.jnucmat.2009.03.010

Nomenclature

K	thermal conductivity (W/cm K)	η	number of available adjacent jump sites
v	volume fraction	υ	vibrational frequency inside lattice (s^{-1})
w	mass fraction	N_{Zr}	zirconium number density in δ-$ZrH_{1.6}$ phase ($atoms/cm^3$)
κ	thermal diffusivity (cm^2/s)	C	H/Zr ratio in ZrH_x
ρ	mass density (kg/cm^3)	T_Q	heat of transport of H in δ-$ZrH_{1.6}$ (K)
C_p	specific heat capacity (J/g K)	S	surface area/volume of shell (cm^{-1})
T	temperature (K)	B	coefficient of expansion of hydrogen
$\dot{q}^m$	volumetric heat generation rate (W/cm^3)	A	coefficient of thermal expansion (K^{-1})
T_{R_f}	fuel surface temperature (K)	ε_r, ε_θ, ε_z	radial, azimuthal, and axial strain
h	heat transfer coefficient (W/cm^2 K)	σ_r, σ_θ, σ_z	radial, azimuthal, and axial stress (MPa)
T_∞	coolant temperature (K)	E	elastic (Young's) modulus (GPa)
δ	cladding/gap thickness (cm)	ν	Poisson's ratio
J	radial flux (cm^{-2}/s)	R	gas constant (kJ/mol K)
D	macroscopic diffusion coefficient (cm^2/s)	k_{DH}	dehydriding rate (mol/cm^2 s)
λ	jump distance during diffusion (cm)		
τ	mean residence time in each lattice site (s)		

retention properties which indicates voids containing noble gases form during operation. This is related to swelling and will further deteriorate the thermal conductivity

$$k_{\text{Fuel}} = k_{\text{U}}\left(v_{\text{U}} + \frac{\kappa_{\text{ZrH}_{1.6}}}{\kappa_{\text{U}}}(1 - v_{\text{U}})\right)\left(v_{\text{U}} + \frac{\rho_{\text{ZrH}_{1.6}}}{\rho_{\text{U}}}(1 - v_{\text{U}})\right)\left(w_{\text{U}} + \frac{C_{p,\text{ZrH}_{1.6}}}{C_{p,\text{U}}}(1 - w_{\text{U}})\right). \quad (1)$$

(Refer to nomenclature for a description and respective units of all the variables discussed in the equations throughout this paper.)

2.1.2. Hydrogen diffusivity

The diffusivity of hydrogen in zirconium hydride has been measured over a relatively large range of temperatures and hydrogen concentrations by Majer et al. [7]. The only set of data corresponding to δ phase zirconium hydride (H/Zr ratio = 1.58) yields the diffusion coefficient as

$$D = 1.53 \times 10^{-3} \exp\left(\frac{-58.8}{RT}\right). \quad (2)$$

The Einstein diffusion model describes the diffusion coefficient as

$$D = \frac{1}{6}\frac{\lambda^2}{\tau}, \quad (3)$$

where λ is the jump distance of the diffusing species and τ is the mean residence time in each site before a jump. The mean residence time is inversely proportional to the product of the number of available adjacent jump sites (η) and the jump frequency. The jump frequency is the product of vibration frequency of the species in that site (υ) with an Arrhenius factor that determines the probability of each vibration leading to a successful jump. Therefore, the pre-exponential factor in the diffusion coefficient can be expressed as

$$D_o = \frac{1}{6}\lambda^2\eta\upsilon, \quad (4)$$

η is the product of the number of adjacent jump sites (6, since hydrogen is on a simple cubic lattice inside the face centered cubic Zr unit cell where the overall structure corresponds to a $Fd\bar{3}m$ space group) with the probability that the site is not currently occupied by another hydrogen atom. This probability can be determined from the stoichiometry and structure of the system; the pre-exponential term can therefore be estimated as

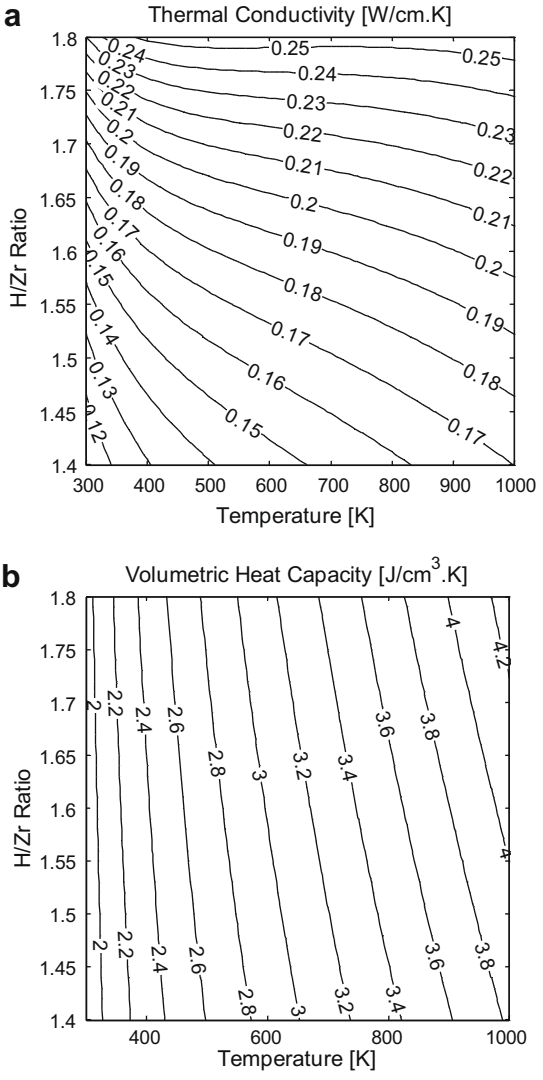

Fig. 1. (a) Thermal conductivity and (b) volumetric heat capacity of the $U_{0.31}ZrH_x$ fuel as functions of temperature and H/Zr ratio.

$$D_o = \frac{1}{6}\lambda^2 6\left(1-\frac{C}{2}\right)\upsilon. \tag{5}$$

Activation energy for diffusion is essentially independent of hydrogen concentration, assuming the mechanism of diffusion does not change in the range of interest (H/Zr ratio from 1.5 to 1.7). The final expression that is used for the diffusion coefficient of hydrogen in δ-ZrH_x is

$$D = 7.29\times10^{-3}\left(1-\frac{C}{2}\right)\exp\left(\frac{-58.8}{RT}\right). \tag{6}$$

2.2. Heat conduction model

The transient radial heat conduction equation for an axial slice of fuel with internal heat generation and variable properties is

$$\frac{\partial}{\partial t}(\rho C_p T) = \frac{1}{r}\frac{\partial}{\partial r}\left(kr\frac{\partial T}{\partial r}\right) + \dot{q}^m. \tag{7}$$

All terms are treated as radially and temporally variant except for the internal heat generation which is approximated as spatially uniform. The validity of this assumption is addressed in detail in the discussion Section 4.3. The steady-state solution defines the initial condition and the time-dependant heat generation drives the model. The two necessary boundary conditions are zero heat flux at the fuel centerline and a fuel surface temperature that depends on the coolant temperature and the conductance between. This second relation is shown below.

$$T_{R_f}(t) = -\frac{k_{R_f}(t)}{h}\left(\frac{\partial T}{\partial r}\right)\Big|_{R_f,t} + T_\infty, \tag{8}$$

where the heat conductance, h, is defined as

$$\frac{1}{h} = R_f\frac{\ln\left(1+\frac{\delta_{gap}}{R_f}\right)}{k_{gap}} + (R_f+\delta_{gap})\frac{\ln\left(1+\frac{\delta_{clad}}{R_f+\delta_{gap}}\right)}{k_{clad}} + \frac{1}{h_{hyd}}. \tag{9}$$

A semi-implicit Crank–Nicolson scheme is used for discretization [8] whereby time is discretized with the trapezoid rule and space with the central difference formula, obtaining inherent stability and second order accuracy. At first glance, the solution might require an iterative predictor-corrector algorithm since the unknown iterate is not known explicitly. However, if the extra effort is made to form the relation into a linear system, the problem is transformed into solving a sparse linear system of equations at each time-step. Fortunately, MATLAB® contains LAPACK, a library of linear algebra subroutines that solves linear systems such as these quickly and accurately. The full discretization of the heat equation can be found in Appendix A.

2.3. Hydrogen diffusion model

The driving force for the flux of hydrogen atoms across the fuel exists due to temperature and concentration gradients across the pellet. The radial flux is equal to

$$J_r = -DN_{Zr}\left(\frac{dC}{dr} + \frac{T_Q C}{T^2}\frac{dT}{dr}\right). \tag{10}$$

After relating the flux and concentration in a conservation equation such as in Huang et al. [9], an explicit time-discretization scheme is used since the rate of change of the concentration is small and linearization introduces only small errors. Flux at the surface of the fuel is approximated to be zero; the accuracy of this simplification is addressed in Section 4. In the conservation equation, the fluxes are multiplied by a ratio of surface area and volume which correspond to the surface through which the flux is passing and the volume of fuel in which hydrogen resides. Since hydrogen exists only in the δ-ZrH_x phase (the flux of hydrogen atoms in the α-U phase is negligible [9]), this area to volume ratio is weighted by the fraction of this phase (~0.9). The fully-expanded discretized diffusion equation and its derivation can be found in Appendix B.

2.4. Coupling algorithm

As mentioned earlier, there is a high degree of interdependency of the pertinent variables. The heat equation for temperature depends on thermal conductivity and volumetric heat capacity. The hydrogen diffusion equation depends on temperature, hydrogen concentration, and diffusivity. The diffusivity, thermal conductivity, and volumetric heat capacity all depend on temperature and hydrogen concentration.

The following operator splitting algorithm is used for each time-step. The heat equation is semi-implicitly solved for the current temperature using properties from the previous time-step and extrapolated properties for the current time-step (see Appendix A). Next, the hydrogen concentration is explicitly calculated for the current time-step using parameters only at the previous time-step (see Appendix B). Third, the diffusivity, thermal conductivity, and volumetric heat capacity are updated with the current temperature and hydrogen concentration. This process is shown in Fig. 2 where arrows denote inputs, circles are variables (dashed lines denote the previous time-step), rectangles are equations, pentagons are boundary conditions, and the hexagon is power density (assumed independent of other variables).

Before the transient solution algorithm is run, the steady-state equations are solved using a similar process with a relative error tolerance for convergence of 10^3 times machine precision.

2.5. Stress calculation

The two sources of strain in the material arise from temperature and hydrogen concentration gradients across the fuel. Olander [10] reported the linear coefficient of expansion of hydrogen as $\beta = 0.027$ per unit change of H/Zr ratio in ZrH_x. The temperature dependent coefficient of thermal expansion of the zirconium hydride has been reported as $\alpha = 3.36\times10^{-6}\,[1 + 4.40\times10^{-3}T]$ per unit change of temperature in Kelvin [11]. The elastic modulus of zirconium hydride is approximately 130 GPa in the temperature range of interest [12]. The elastic modulus of the composite fuel is obtained using the rule of mixtures as 145 GPa (vol% α-U = 19.4). With a similar analysis, the Poisson ratio for the composite is 0.3 ($\nu_{\alpha\text{-U}} = 0.23$, $\nu_{ZrH_{1.6}} = 0.32$ [12]). Total strain in the fuel is the sum of elastic, thermal and hydrogen strains. The constitutive

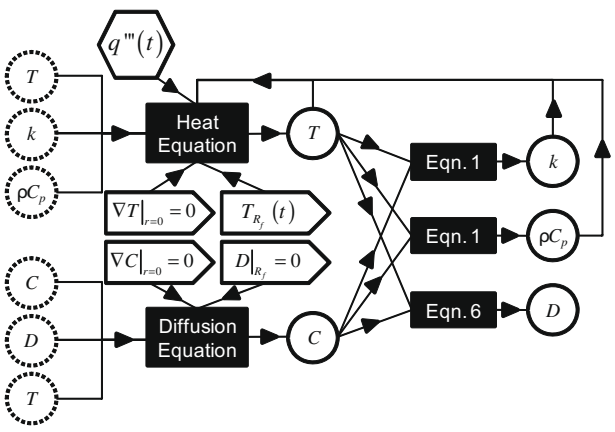

Fig. 2. A single time-step in the solution algorithm.

equations in the axi-symmetric cylindrical coordinates are then presented as

$$\varepsilon_r = \frac{1}{E}[\sigma_r - \nu(\sigma_\theta + \sigma_z)] + \alpha(\Delta T) + \beta(\Delta C), \quad (11)$$

$$\varepsilon_\theta = \frac{1}{E}[\sigma_\theta - \nu(\sigma_r + \sigma_z)] + \alpha(\Delta T) + \beta(\Delta C), \quad (12)$$

$$\varepsilon_z = \frac{1}{E}[\sigma_z - \nu(\sigma_\theta + \sigma_r)] + \alpha(\Delta T) + \beta(\Delta C). \quad (13)$$

Eliminating the displacement vectors in the definition of cylindrical strains, the relationship in Eq. (14) is obtained. Using the constitutive equations coupled with this condition and also assuming a plane strain scenario in the axial direction, a differential equation governing the radial stress across the fuel is determined (Eq. (15)). The fuel is assumed initially restrained in the axial direction (the plain strain assumption); later by application of Saint Venant's principle the unrestrained axial stress is determined [13]. The two necessary boundary conditions are a zero stress gradient at the fuel centerline and zero radial stress at the fuel surface

$$\frac{d\varepsilon_\theta}{dr} + \frac{\varepsilon_\theta - \varepsilon_r}{r} = 0, \quad (14)$$

$$\frac{1}{r^2}\frac{d}{dr}\left(r^3\frac{d\sigma_r}{dr}\right) = \frac{-E}{1-\nu}\left[\frac{d}{dr}(\alpha T) + \beta\frac{dC}{dr}\right]. \quad (15)$$

The radial equilibrium condition in cylindrical coordinates (Eq. (16)) is used to calculate the azimuthal stress across the fuel based on the radial stress

$$\sigma_\theta = \frac{\partial}{\partial r}(r\sigma_r). \quad (16)$$

To determine the distribution of axial stress across the fuel, the axial stress is first calculated assuming complete restraint in the axial direction ($\varepsilon_z = 0$). Then the difference from the average of this quantity across the fuel is denoted as the actual magnitude of axial stress (Saint Venant's principle). For the complete set of calculations showing the derivation of different stress components please refer to Appendix C.

Simpson and Cann [14] report the mode I fracture toughness of δ-zirconium hydride as 3 MPa $m^{1/2}$ at 573 K. Ductile phase toughening in the fuel due to the presence of uranium particles is expected by crack bridging and process zone toughening mechanisms. By conservatively ignoring such effects, linear elastic fracture mechanics can be applied. However finite element methods are necessary to predict the evolution of flaw size in the material due to the complex state and distribution of stress and are beyond the scope of this work. An adequate scheme would be to artificially assign cracks to different regions of the material that would in turn correspond to dissimilar states of stress. The progression in flaw size and geometry that correspondingly depends on the evolution of the changing stress state can then be studied.

2.6. Model physical parameters

The model was composed of a fuel element 1 cm in diameter, housed inside a zircaloy cladding of 0.9 mm in thickness, with a 70 μm molten lead–tin–bismuth (Pb-33.3 wt%Sn-33.3 wt%Bi) gap in between. The gap and cladding were not modeled explicitly but instead were introduced as the outer boundary condition along with the hydraulic conditions. The conductivities used for the liquid–metal (LM) gap and clad were 0.20 W/cm K [15] and 0.16 W/cm K [16], respectively. The thermal-hydraulic heat transfer coefficient was estimated using the Presser correlation for the Nusselt number with the typical geometry and operating parameters of a PWR, resulting in an approximate value of 1 W/cm^2 K. The bulk coolant temperature was 575 K and the pitch to diameter ratio was 1.2. The fuel-averaged H/Zr ratio was 1.6.

3. Results

3.1. Steady-state results

The steady-state calculations were conducted with 500 spatial nodes at linear heat rates (LHR) of 100, 200, and 300 W/cm. The

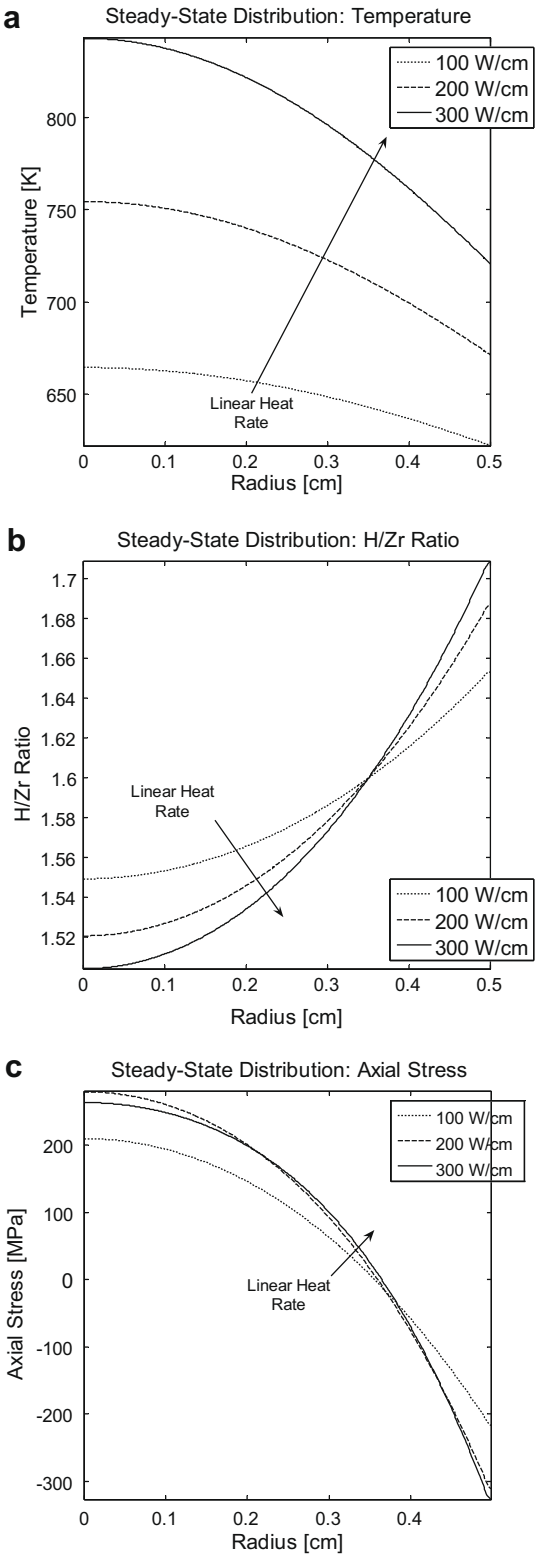

Fig. 3. (a) Steady-state temperature, (b) H/Zr ratio, and (c) axial stress distributions at LHRs of 100, 200, and 300 W/cm.

results of the steady-state temperatures, H/Zr ratios, and axial stress distributions are shown in Fig. 3(a)–(c), respectively.

As expected, the fuel temperature gradient and outer fuel temperature increase with LHR. The hydrogen concentration gradients are also steeper with increasing LHR. With a LM bonded fuel, even though the average temperature is lower when compared to the conventional He gap fuel, the extent of hydrogen redistribution is more severe (as reported by Olander [10]). This has been confirmed by the model but is not shown in this paper. This trend is justified by inspection of the flux governing equation where the T^{-2} dependence of the temperature gradient term enhances its impact at lower temperatures.

The largest component of stress is the axial stress, whose value is influenced by the temperature and hydrogen concentration gradients in an opposing manner. However, hydrogen-induced stresses are the dominant component, as is evident from the steady-state results. Generally, the fuel surface experiences severe compression from axial and azimuthal components of stress, while all three components of stress are tensile at the central region of the fuel. Even though the hydrogen redistribution is larger with increasing LHR, the magnitude of stress might not increase due to larger thermally induced strains.

3.2. Transient results

A parametric transient case study was completed with a nominal LHR and coolant temperature of 300 W/cm and 575 K, respectively. The power was pulsed to twice the nominal value for 2.5 s and then dropped to 5% while the coolant temperature and fuel-to-coolant conductance remained constant. This represents a simplified and exaggerated reactivity insertion accident (RIA) with a large pulse height, a long pulse width, and a subsequent SCRAM. The hydrogen redistribution, although present, is miniscule since the hydrogen diffusivity is orders of magnitude smaller than the thermal diffusivity ($\sim 2 \times 10^{-8}$ cm^2/s compared to $\sim 6 \times 10^{-2}$ cm^2/s). Consequently, only the resultant spatial fuel temperature and axial stress distributions are shown in Fig. 4(a) and (b), respectively.

The fuel temperature directly follows the power pulse, rapidly peaking as the power jumps and then relaxing down after the SCRAM. The stress response of the fuel is interesting in that the axial stress is actually lowered and flattened during the power pulse. This is caused by the increased thermal stresses that counteract the dominating stresses created by the hydrogen concentration gradient. As the fuel cools during the SCRAM portion, the hydrogen-induced stresses remain unopposed and the overall stress increases. Fig. 5 shows the maximum fuel temperature for various pulse heights and durations induced on a fuel operating with nominal linear heat rate of 300 W/cm.

4. Discussion

4.1. Comparison of constant to variable properties

Table 1 summarizes the relative percent error one would accrue by using material properties that are independent of temperature and hydrogen concentration for a steady-state solution. The constant values used for thermal conductivity and volumetric heat capacity were 0.16 W/cm K and 2.3 J/cm^3 K. Results are shown for LHRs of 100, 200, and 300 W/cm.

Although the relative percent errors may seem small, a 3% relative difference amounts to 30 K at a temperature of 1000 K. Also, at 100 W/cm, the overshoot in temperature and undershoot in H/Zr ratio at the fuel centerline would bring about a significant error in the axial stress. A moderate discrepancy in any of these terms may have a significant effect on the overall fuel behavior.

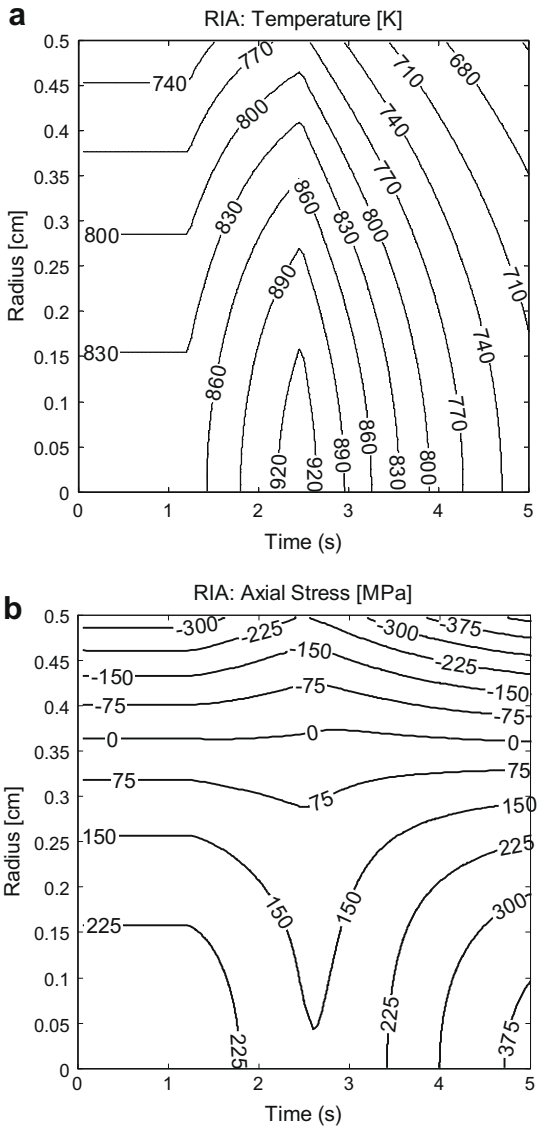

Fig. 4. (a) Fuel temperature and (b) axial stress response to RIA.

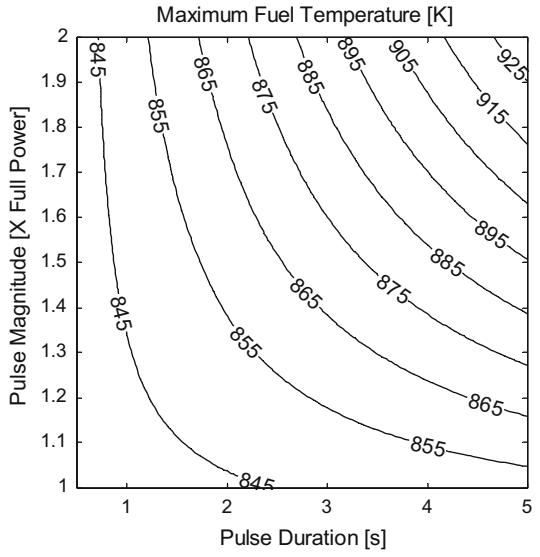

Fig. 5. Maximum fuel temperature during power pulse.

Table 1
Effects of variable property versus constant property analyses: relative error.

LHR (W/cm)	Maximum temperature (%)	H/Zr at fuel center (%)	H/Zr at fuel surface (%)	Axial stress at fuel center (%)
100	1.11	−0.51	0.55	12
200	2.18	−0.84	0.97	8.73
300	3.19	−1.05	1.29	2.78

4.2. Extent and effect of hydrogen desorption

The extent of hydrogen release from the LM bonded fuel is unknown. However, it is believed to be smaller when compared to the case of fuel gap filled with helium, since the hydrogen is readily released from the surface into a much larger volume and the gas phase solubility is infinite. For perspective, it is appropriate to study fuel with a He filled gap. The extent of release can then be estimated by the equilibrium partial pressure of hydrogen inside the cladding, which can be expressed as a function of temperature and fuel surface hydrogen concentration according to Wang et al. [17] as

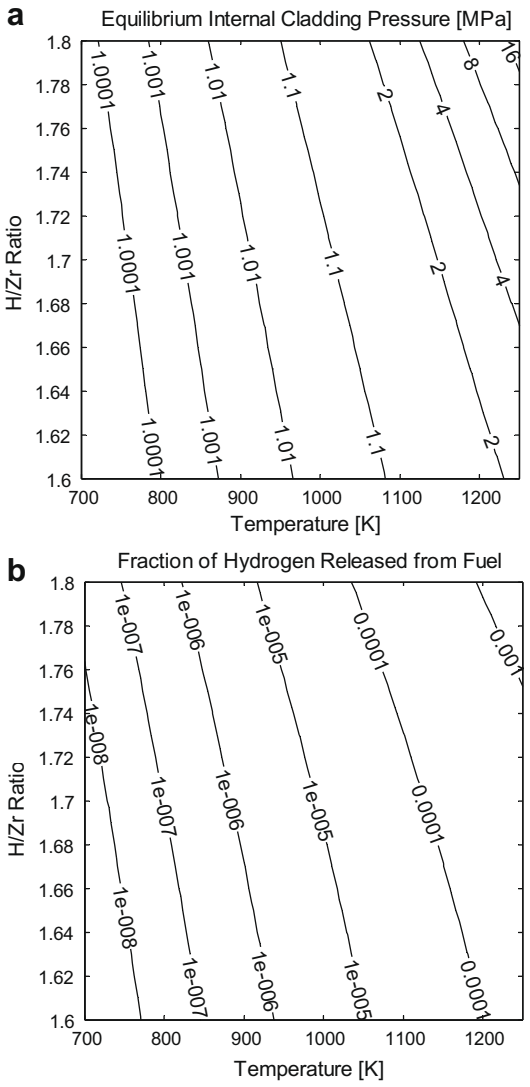

Fig. 6. (a) Equilibrium total pressure inside the cladding (MPa). (b) Total fraction of hydrogen inside the fuel lost to the gaseous phase inside the cladding in equilibrium.

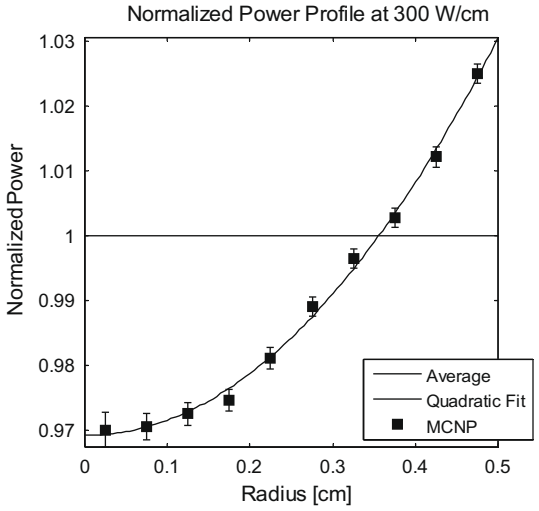

Fig. 7. Distribution of the power profile across the fuel operated at 300 W/cm linear heat rate.

$$P(\text{atm}) = \left(\frac{C_{eq}}{2 - C_{eq}}\right)^2 \exp\left(8.01 + 5.21C_{eq} - \frac{2.07 \times 10^4}{T(\text{K})}\right). \quad (17)$$

The free volume inside the cladding due to the plenum volume and gap is approximately 40 cm^3. Assuming a pre-pressurization to 1 MPa of He, the total pressure in the cladding can be calculated as the sum of partial pressures of hydrogen and helium that in turn obey the ideal gas law. Therefore equilibrium pressure inside the cladding as function of temperature and H/Zr ratio at the fuel surface could be estimated as shown in Fig. 6(a). The plenum and gap are conservatively assumed to be at the fuel surface temperature. The amount of hydrogen within each fuel rod is approximately 25 mol. The equilibrium fractional loss of this amount as function of fuel surface temperature and H/Zr ratio at the fuel surface is also shown in Fig. 6(b). Adsorption of hydrogen on the inner surface of cladding and its subsequent diffusion into the cladding is ignored. Over time however, this will result in a larger fractional release of hydrogen into the cladding.

4.3. Magnitude and effect of power depression

A pin cell model was built in MCNP (Monte Carlo N-Particle Transport Code) to determine the steady-state power profile during the reactor operation so the accuracy of the uniform power approximation could be addressed. The steady-state temperature and hydrogen concentration results with the uniform power LHR of 300 W/cm were used as input for the cross-sections and number densities of the MCNP model. The power was tallied in 10 radial shells of the fuel. The resultant power profile was used to update the heat and hydrogen diffusion model and the process was iterated until convergence. The normalized power profile for the first iteration is shown in Fig. 7. The maximum difference between the uniform and depressed power profiles is around 2% and it changes the centerline temperature by 2.25 K, or ~0.8% of the fuel centerline to coolant temperature drop. Its effects on the hydrogen concentration and stresses are even smaller, leaving one to conclude that the uniform power profile is a good assumption.

5. Conclusions

Steady state and transient behavior of several aspects of the fuel operating performance have been investigated, taking into account the temperature and hydrogen concentration dependence of the fuel properties.

Steady-state temperature, hydrogen concentration, and stress profiles of the hydride fuel operated at various linear heat rates have been calculated. The extent of hydrogen redistribution, driven by the gradient in temperature, becomes more severe as the power increases. Strains in the fuel occur from thermal and hydrogen concentration gradients, with the latter being the dominant contributor. Axial and azimuthal stresses are both compressive at the surface and tensile at the fuel centerline. These results are in agreement with what was previously shown by Olander, where the dependence of fuel properties (except the coefficient of thermal expansion) on temperature and hydrogen concentration were ignored [10]. The fuel fracture criterion is unknown and needs be determined through finite element methods.

The transient response of hydride fuel to a reactivity insertion accident scenario was studied by artificially pulsing power in a square wave. The thermal response of the fuel to the changing boundary conditions is very rapid (on order of few seconds) due to the small fuel rod and large thermal diffusivity. There is no discernable alteration in the transient hydrogen profile, since the characteristic diffusion time for these length scales is many orders of magnitude larger than the transient durations. However, it is necessary to model the hydrogen diffusion since it is important to know the steady-state distribution for the initial conditions. Surprisingly, the stress across the fuel is actually reduced during the power pulse. The temperature-induced stresses counteract the hydrogen-induced stresses, so the fuel is in its most relaxed state during this stage of the transient. The fuel experiences maximum stress when temperature gradients diminish but the hydrogen displacement remains at the pre-transient distribution.

The flux of hydrogen atoms, in a fuel assembly with a He filled gap, out of the fuel during steady state and transient operation of the fuel is very small since the net rate (desorption–adsorption) quickly becomes zero when the equilibrium hydrogen partial pressure is established. The pressure buildup inside the cladding and the total fraction of hydrogen lost from the solid state to the cladding volume are negligible even at very high fuel surface temperatures. The extent of dehydriding is expected to be even less for LM bonded fuels.

Acknowledgements

The authors wish to thank Professor Per Peterson for helpful discussions and comments.

Appendix A

The radial heat equation with variable properties is a non-linear partial differential equation (Eq. (7)), so discretization must be done carefully. A well known procedure is that of Crank and Nicolson [8], in which time is discretized with the trapezoid rule and space with central difference. This first step is shown below:

$$\begin{aligned}&\frac{1}{\Delta t}((\rho C_p T)_i^{j+1}-(\rho C_p T)_i^j)\\&=\frac{1}{2}\left(\dot{q}_i^{mj+1}+\dot{q}_i^{mj}\right)+\frac{1}{2}\frac{1}{r_i\Delta r}\left[\left(rk\frac{\partial T}{\partial r}\right)_{r_{i+1/2}}^{j+1}-\left(rk\frac{\partial T}{\partial r}\right)_{r_{i-1/2}}^{j+1}\right.\\&\left.+\left(rk\frac{\partial T}{\partial r}\right)_{r_{i+1/2}}^{j}-\left(rk\frac{\partial T}{\partial r}\right)_{r_{i-1/2}}^{j}\right],\end{aligned}\tag{A1}$$

where i and j indicate the radial node and time-step, respectively. All terms are considered as node-centered. The equation is expanded and shuffled more:

$$\begin{aligned}&\left((\rho C_p)_i^{j+1}T_i^{j+1}-(\rho C_p)_i^jT_i^j\right)\\&=Q\Delta t+\omega\left[\frac{r_{i+1/2}}{r_i}k_{i+1/2}^{j+1}\left(T_{i+1}^{j+1}-T_i^{j+1}\right)\right.\\&-\frac{r_{i-1/2}}{r_i}k_{i-1/2}^{j+1}(T_i^{j+1}-T_{i-1}^{j+1})+\frac{r_{i+1/2}}{r_i}k_{i+1/2}^{j}(T_{i+1}^{j}-T_i^{j})\\&\left.-\frac{r_{i-1/2}}{r_i}k_{i-1/2}^{j}(T_i^{j}-T_{i-1}^{j})\right],\end{aligned}\tag{A2}$$

where the following terms and notations are defined and used for convenience:

$$Q=\frac{1}{2}(\dot{q}_i^{mj+1}+\dot{q}_i^{mj}),\tag{A3}$$

$$\omega=\frac{\Delta t}{2\Delta r^2},\tag{A4}$$

$$k_{i\pm1/2}=\frac{1}{2}(k_{i\pm1}+k_i).\tag{A5}$$

Since a marching procedure is performed with time, solving for the $j+1$st iterate from the known jth iterate, the thermal conductivity and volumetric heat capacity at the $j+1$st time-step are not known as they depend on both temperature and hydrogen concentration. Further, the functional dependencies are highly non-linear. Initially, predictor-corrector iterations were performed at each time-step, requiring substantial increases in run-time. Newton–Raphson methods were also considered but were deemed too laborious. A final, simpler method that produces results with essentially no difference is a first-order Taylor extrapolation of the material properties using the jth and $j-1$st values. This procedure is outlined below:

$$k^{j+1}\approx k^j+\Delta t\frac{\partial k^j}{\partial t}\approx k^j+\Delta t\frac{k^j-k^{j-1}}{\Delta t}=2k^j-k^{j-1},\tag{A6}$$

$$(\rho c_p)^{j+1}\approx 2(\rho c_p)^j-(\rho c_p)^{j-1}.\tag{A7}$$

The node-centered radius terms are also expanded accordingly:

$$r_i=\Delta r(i-1/2),\tag{A8}$$

$$\frac{r_{i\pm1/2}}{r_i}=\frac{r_{i\pm\Delta r/2}}{r_i}=1\pm\frac{\Delta r}{2r_i}=1\pm\frac{\Delta r}{2\Delta r(i-1/2)}=1\pm\frac{1}{2i-1}.\tag{A9}$$

Utilizing these enhancements, the final form of the semi-implicitly discretized heat equation is acquired:

$$\begin{aligned}&\left\{\begin{array}{l}T_i^{j+1}\left[\frac{(\rho c_p)_i^{j+1}}{\omega}+\left(1+\frac{1}{2i-1}\right)k_{i+1/2}^{j+1}+\left(1-\frac{1}{2i-1}\right)k_{i-1/2}^{j+1}\right]\\+T_{i+1}^{j+1}\left[-\left(1+\frac{1}{2i-1}\right)k_{i+1/2}^{j+1}\right]+T_{i-1}^{j+1}\left[-\left(1-\frac{1}{2i-1}\right)k_{i-1/2}^{j+1}\right]\end{array}\right\}\\&=\left\{\begin{array}{l}T_i^{j}\left[\frac{(\rho c_p)_i^{j}}{\omega}-\left(1+\frac{1}{2i-1}\right)k_{i+1/2}^{j}-\left(1-\frac{1}{2i-1}\right)k_{i-1/2}^{j}\right]\\+T_{i+1}^{j}\left[\left(1+\frac{1}{2i-1}\right)k_{i+1/2}^{j}\right]+T_{i-1}^{j}\left[\left(1-\frac{1}{2i-1}\right)k_{i-1/2}^{j}\right]\end{array}\right\}+\frac{Q\Delta t}{\omega}.\end{aligned}\tag{A10}$$

Appendix B

The hydrogen mass balance equation can be written for a differential radial shell in terms of the flux within the fuel as the following:

$$c_i^{j+1}=c_i^j+[J_{i-1/2}^jS_{i-1/2}-J_{i+1/2}^jS_{i+1/2}]\Delta t,\tag{B1}$$

where c is the molar concentration of hydrogen in mole H/cm^3; J is the hydrogen atom flux specified earlier in Eq. (10). S is the ratio of inner/outer surface of each radial shell to its volume with units of cm^{-1}:

$$S_{i\pm1/2}=\frac{2\pi r_{i+1/2}l}{\pi(r_{i+1/2}^2-r_{i-1/2}^2)l}=\frac{2(r_i\pm\Delta r/2)}{([r_i+\Delta r/2]^2-[r_i-\Delta r/2]^2)}.\tag{B2}$$

After substituting Eq. (A9) and simplifying, (B2) becomes:

$$S_{i\pm1/2}=\frac{2(r_i\pm\Delta r/2)}{(2r_i\Delta r)}=\frac{r_i\pm\Delta r/2}{r_i\Delta r}\overset{r_i=\Delta r(i-1/2)}{\rightarrow}\begin{cases}-\rightarrow\frac{i-1}{\Delta r(i-1/2)}\\ +\rightarrow\frac{i}{\Delta r(i-1/2)}\end{cases}. \tag{B3}$$

The atomic ratio of hydrogen to zirconium is:

$$C_i^j=\frac{M_{Zr}}{\rho_{Zr}}c_i^j. \tag{B4}$$

Substituting for Eqs. (B3), (B4), (10), and (B1) generates the following result:

$$\begin{aligned}C_i^{j+1}\frac{\rho_{Zr}}{M_{Zr}}=C_i^j\frac{\rho_{Zr}}{M_{Zr}}+\Bigg[&-D_{i-1/2}^j\frac{\rho_{Zr}}{M_{Zr}}\left\{\frac{C_i^j-C_{i-1}^j}{r_i-r_{i-1}}+\frac{T_QC_{i-1/2}^j}{T_{i-1/2}^2}\cdot\frac{T_i-T_{i-1}}{r_i-r_{i-1}}\right\}\\ &\times\frac{i-1}{\Delta r(i-1/2)}+D_{i+1/2}^j\frac{\rho_{Zr}}{M_{Zr}}\left\{\frac{C_{i+1}^j-C_i^j}{r_{i+1}-r_i}+\frac{T_QC_{i+1/2}^j}{T_{i+1/2}^2}\cdot\frac{T_{i+1}-T_i}{r_{i+1}-r_i}\right\}\\ &\times\frac{i}{(i+1/2)\Delta r}\Bigg]\Delta t.\end{aligned} \tag{B5}$$

Further simplification of the above results in the fully explicit discretization for H/Zr ratio as

$$\begin{aligned}C_i^{j+1}=C_i^j&\left[1-0.9\frac{\Delta t}{\Delta r^2}D_{i+1/2}^j\frac{i}{(i+1/2)}\left\{1-\frac{T_Q(T_{i+1}^j-T_i^j)}{2\left(T_{i+1/2}^j\right)^2}\right\}\right.\\ &\left.-0.9\frac{\Delta t}{\Delta r^2}D_{i-1/2}^j\frac{i-1}{(i-1/2)}\left\{1+\frac{T_Q(T_i^j-T_{i-1}^j)}{2\left(T_{i-1/2}^j\right)^2}\right\}\right]\\ &+C_{i+1}^j\left[0.9\frac{\Delta t}{\Delta r^2}D_{i+1/2}^j\frac{i}{(i+1/2)}\left\{1+\frac{T_Q(T_{i+1}^j-T_i^j)}{2\left(T_{i+1/2}^j\right)^2}\right\}\right]\\ &+C_{i-1}^j\left[0.9\frac{\Delta t}{\Delta r^2}D_{i-1/2}^j\frac{i-1}{(i-1/2)}\left\{1-\frac{T_Q(T_i^j-T_{i-1}^j}{2\left(T_{i-1/2}^j\right)^2}\right\}\right].\end{aligned} \tag{B6}$$

Appendix C

Eq. (15) for the radial stress is first discretized with central difference:

$$\begin{aligned}&\frac{1}{r_i^2}\frac{1}{\Delta r}\left(r^3\frac{d\sigma_r}{dr}\Big|_{r_{i+1/2}}-r^3\frac{d\sigma_r}{dr}\Big|_{r_{i-1/2}}\right)\\ &=\frac{-E}{1-\nu}\left[\frac{1}{\Delta r}\left(\alpha T|_{r_{i+1/2}}-\alpha T|_{r_{i-1/2}}\right)+\beta\frac{C_{i+1/2}-C_{i-1/2}}{\Delta r}\right].\end{aligned} \tag{C1}$$

Utilizing Eqs. (A8) and (A9) and taking into account the linearly temperature dependant coefficient of thermal expansion Eq. (C1) becomes:

$$\begin{aligned}&\sigma_{r,i}\left(-i\left[1+\frac{1}{2i-1}\right]^2-(i-1)\left[1+\frac{1}{2i-1}\right]^2\right)\\ &+\sigma_{r,j+1}\left(i\left[1+\frac{1}{2i-1}\right]^2\right)+\sigma_{r,j+1}\left((i-1)\left[1-\frac{1}{2i-1}\right]^2\right)\\ &=\frac{-E}{1-\nu}\left[\alpha_o\left(\left[T_{i+1/2}-T_{i-1/2}\right]+a\left[T_{i+1/2}^2-T_{i-1/2}^2\right]\right)+\frac{\beta}{2}(c_{i+1}-C_{i-1})\right].\end{aligned} \tag{C2}$$

With the boundary conditions described in Section 2.5, Eq. (C2) can be solved in the matrix form, obtaining the radial stress across the fuel. The azimuthal stress across the fuel is then determined through Eq. (16) as the following, where the condition of radially symmetric stress is again applied:

$$\sigma_{\theta,i}=\frac{1}{2}\left(i(\sigma_{r,i+1}+\sigma_{r,i})-(i-1)(\sigma_{r,i}+\sigma_{r,i-1})\right). \tag{C3}$$

As discussed in Section 2.5 the axial stress is defined as the difference between the actual to the mean of the restrained axial stress (such that $\varepsilon_z = 0$), as shown in Eq. (C4)

$$\sigma_{z,i}=\sigma_{z,i}^R-\bar{\sigma}_{z,i}^R. \tag{C4}$$

The actual and mean of the restrained axial stress are found as shown in Eqs. (C5) and (C6). The reference temperature was taken as 750 K, corresponding to the typical fuel processing temperatures, during which the material is assumed to be free of residual stresses. The reference value of H/Zr ratio is 1.6.

$$\begin{aligned}\sigma_{z,i}^R=\nu(\sigma_{\theta,i}+\sigma_{r,i})-E[(\alpha_\circ[T_i+aT_i^2]-\alpha_\circ[T_{\text{ref}}+aT_{\text{ref}}^2])\\ +\beta(C_i-C_{\text{ref}},)]\end{aligned} \tag{C5}$$

$$\bar{\sigma}_{z,i}^R=\frac{2}{R^2}\int_0^R r\sigma_{z,r}^R dr=\frac{2}{R^2}\sum_{i=1}^m(i-1/2)\sigma_{z,i}^R\Delta r^2. \tag{C6}$$

References

[1] F. Ganda, E. Greenspan, Plutonium incineration capability of hydride versus MOX fuel in PWR, in: Proceedings of the Global '05, Tsukuba, Japan, October 2005.
[2] A. Sommer, W. Dennison, NAA-SR-5066, 1960.
[3] S. Yamanaka, K. Yamada, K. Kurosaki, M. Uno, K. Takeda, H. Anada, T. Matsuda, S. Kobayashi, J. Nucl. Mater. 294 (2001) 94.
[4] Y. Takahashi, M. Yamawaki, K. Yamamoto, J. Nucl. Mater. 154 (1988) 141.
[5] I. Grenthe, J. Fuger, R. Konings, R. Lemire, A. Muller, C. Nguyen-Trung, H. Wanner, Chemical Thermodynamics of Uranium, OECD Publications, Paris, France, 2004.
[6] B. Tsuchiya, J. Huang, K. Konashi, M. Teshigawara, M. Yamawaki, J. Nucl. Mater. 289 (2001) 329.
[7] G. Majer, W. Renz, R. Barnes, J. Phys.: Condens. Matter (1994) 2935.
[8] J. Crank, P. Nicolson, Proc. Camb Philos Soc. 43 (1947) 50.
[9] J. Huang, B. Tsuchiya, K. Konashi, M. Yamawaki, J. Nucl. Sci. Technol. 37 (2000) 887.
[10] D. Olander, M. Ng, J. Nucl. Mater. 346 (2005) 98.
[11] M. Simnad, Nucl. Eng. Des. 64 (1981) 403.
[12] S. Yamanaka, K. Yoshioka, M. Uno, M. Katsura, H. Anada, T. Matsuda, S. Kobayashi, J. Alloys. Compd. 293–295 (1999) 23.
[13] H. Rust, Nucl. Power Plant Eng. (1979) 393.
[14] L. Simpson, C. Cann, J. Nucl. Mater. 87 (1979) 303.
[15] Y. Kim, D. Olander, S. Yagnik, Nucl. Technol. 128 (1999) 300.
[16] J. Fink, Zircaloy Thermal Conductivity: Preliminary Recommendation, International Nuclear Safety Center, Argonne National Laboratory. Available from: <http://www.insc.anl.gov/matprop/zircaloy/zirck.pdf>, 2000.
[17] W. Wang, D. Olander, J. Am. Ceram. Soc. 78 (1995) 3323.